Journal of Colloid and Interface Science 394 (2013) 147–156

Contents lists available at SciVerse ScienceDirect

Journal of Colloid and Interface Science

www.elsevier.com/locate/jcis

A new synthesis pathway for colloidal silica spheres coated with crystalline titanium oxide and its comparative cyto- and genotoxic study with titanium oxide nanoparticles in rat osteosarcoma (UMR106) cells

A.L. Di Virgilio [a], I. Maisuls [b], F. Kleitz [c], P.M. Arnal [b,*]

[a] CEQUINOR and Cátedra de Bioquímica Patológica, Facultad de Ciencias Exactas, UNLP. 47 y 115 (1900) La Plata, Argentina
[b] CETMIC (Centro de Tecnología de Recursos Minerales y Cerámica), Cno Centenario y 506, CC 49 (B1897ZCA), M.B. Gonnet, Prov. Buenos Aires, Argentina
[c] Department of Chemistry and Centre de Recherche Sur les Matériaux Avancés (CERMA), Université Laval, Quebec City, QC, Canada G1V 0A6

ARTICLE INFO

Article history:
Received 31 August 2012
Accepted 5 November 2012
Available online 29 November 2012

Keywords:
Core@shell materials
Nanoparticles
Toxicity
Titanium oxide
Silica
Anatase
Mesopores
Osteoblast cells culture

ABSTRACT

Spherical particles with an amorphous core of silica and a crystalline shell of titanium oxide (SiO_2@TiO_2) formed in a three-step procedure, being the last step a mild chemical treatment. SiO_2@TiO_2 had a shell with pores (micro and mesopores) permeating between TiO_2 nanocrystals (anatase) and a solid core of amorphous silica. The spheres had an outstanding specific surface area (300 $m^2\,g^{-1}$). A cyto- and genotoxic study of SiO_2@TiO_2 and titanium oxide nanoparticles (TiO_2-NP) on UMR106 cells with 24 h exposure showed that SiO_2@TiO_2 colloidal particles were less toxic than TiO_2-NP.

© 2012 Elsevier Inc. All rights reserved.

1. Introduction

Fine particles with a characteristic size smaller than 100 nm (i.e., nanoparticles) as well as fine particles with a characteristic size within the range 100 nm–1 μm (i.e., colloidal particles) spread out in nowadays life. They constitute commercially available products such as cosmetics, participate in medical diagnostics and treatments, and are used in agriculture.

Among them stands out a group, which common characteristic is to have both one material at the core and another material at the shell (i.e., core@shell particles). These core@shell particles attracted the interests of the scientific community, because of their potential biomedical applications in drug delivery and bioimaging as well as in bioelectronics and water cleaning, among others [1–5].

Core@shell particles having an amorphous, solid core of SiO_2 and a crystalline, porous shell of TiO_2 (i.e., SiO_2@TiO_2) are interesting candidates for removing organic contaminants from water. One reason is that titanium oxide (TiO_2) is a well-known photo-catalyst for decomposing organic molecules present in water [6]. Many organic compounds polluting water can be converted into CO_2 with TiO_2 and UV light [7]. Furthermore, SiO_2@TiO_2 particles with crystalline shell have been investigated, for instance, as photocatalysts for the photodegradation of Rhodamine B [8] and methylene blue [9]. A second reason is that colloidal SiO_2@TiO_2 particles may be less harmful to biological systems than TiO_2 nanoparticles. At any given composition, nanoparticles may be more harmful to biological systems than granular material with sizes somewhere above the nano-domain up to sands (i.e., particles with diameters somewhere between 100 nm and 100 μm) [10–14]. Moreover, harm caused by nanoparticles may depend on their size as well as on their shape and surface functionality suggesting that the interaction between surfaces of nanomaterials and cells may play a key role regarding their toxic effects [15]. Even titanium dioxide, long considered to be biologically inert [16,17], rose more recently serious concerns, because of its potential risks when present in the form of nanoparticles [18–21].

SiO_2@TiO_2 has been synthesized using SiO_2 spheres as templates by diverse pathways. One synthesis pathway proceeded via heterocoagulation of silica spheres and titania nanosol [8]. Another one built SiO_2@TiO_2 particles via layer-by-layer self-assembly of cationic polyelectrolyte and anionic titania nanosheets [22]. In a third approach, SiO_2@TiO_2 particles formed after mixing $Ti(OCH_2CH_3)_4$ dissolved in ethanol and silica spheres in a solution of water, ethanol, and hydroxipropyl cellulose [23]. In a different procedure, silica

* Corresponding author. Fax: +54 221 471 00 75.
E-mail address: arnal@cetmic.unlp.edu.ar (P.M. Arnal).

0021-9797/$ - see front matter © 2012 Elsevier Inc. All rights reserved.
http://dx.doi.org/10.1016/j.jcis.2012.11.005

spheres and $Ti(OCH_2CH_2CH_2CH_3)_4$ were first dispersed in an aqueous ethanol solution, then water and ammonium hydroxide were added to the suspension by continuous feeding for about 4 h, the colloid was refluxed for 1.5 h and finally stirred for another 1.5 h to form $SiO_2@TiO_2$ particles. While in the first synthesis pathway crystallization of TiO_2 occurred before the synthesis of core@shell, in all other synthesis pathways crystallization of titanium oxide was brought about by thermal treatment a posteriori.

With regard to their biocompatibility, both nano and colloidal core@shell particles have been evaluated with different biological systems both *in vitro* and *in vivo*. The toxicity of nanoparticles has been analyzed using different cell lines. $AlCl_3$ nanoparticles increased micronuclei [24] and damaged DNA [25]. TiO_2 nanoparticles induced sister chromatid exchanges and micronuclei in Chinese hamster ovary—K1 cells [26]. Silver nanoparticles provoked cyto- and genotoxic damage in human mesenchymal stem cells. Comet assay and chromosomal aberration tests showed DNA damage at concentrations as low as 0.1 ppm [27]. Finally, reduced graphene oxide nanoplatelets produced genotoxic effects through DNA fragmentation and chromosomal aberrations in the same cells [28].

Strict comparison of different *in vitro* and *in vivo* studies of core@shell particles is difficult, because of the formation of a "protein corona" at the particle's surface [29,30]. A protein corona forms by adsorption of biomolecules such as proteins and lipids. It usually contains 10–50 proteins that have the highest affinity for the surface, while several thousand proteins are present in human biological fluids. Its formation is a complex dynamic process that depends not only on physicochemical properties of the solid particles, but also on the composition of the biofluid they are immersed in. Hence, biocompatibility ought to evaluate on a case-by-case basis.

$SiO_2@TiO_2$ particles stand out from other materials as a candidate in photocatalysis. However, $SiO_2@TiO_2$ synthesized so far had relatively low specific surface areas, and their biocompatibility was not reported. Hence, this work presents a new synthesis pathway to obtain silica spheres coated with TiO_2 nanocrystals (anatase) having a specific surface area around $300\ m^2.g^{-1}$. In addition, this work presents a comparative study on the toxicological effects with TiO_2 nanoparticles (anatase) in osteoblast-like cells (UMR106).

2. Experimental

2.1. Materials

This work used following materials and chemicals. *Synthesis of $SiO_2@TiO_2$*. Lutensol AO5 solution was prepared with 11.01 g MQ water and 0.45 g Lutensol AO5. Absolute ethanol, ammonia solution in water, distilled water, tetrabutyl ortotitanate, concentrated HCl, and tetraethyl ortosilicate (*TEOS*). TiO_2-NP (anatase) was purchased from Aldrich (Milwaukee, WI, USA). *Biocompatibility studies*. Tissue culture materials were purchased from Trading New Technologies (Buenos Aires, Argentina). Dulbecco's Modified Eagles Medium (DMEM) was purchased from GBO Argentina, fetal bovine serum (FBS) from Internegocios SA (Buenos Aires, Argentina); trypsin-EDTA was provided by Gibco (Gaithersburg, Md, USA); MTT, Neutral Red dye, Trypan Blue and cytochalasin B from *Dreschslera dematioidea* were purchased from Sigma Chemical Co. (St. Louis, MO, USA). Dihydrorhodamine 123 (DHR) was from Molecular Probes (Eugene, OR, USA). Bleomycin (*BLM*) (Blocamycin®) was kindly provided by Gador S.A. (Buenos Aires, Argentina). Syber Green and Low melting point agarose were purchased from Invitrogen Corporation (Buenos Aires, Argentina). Stock suspensions of TiO_2-NP and $SiO_2@TiO_2$ were prepared in phosphate-buffered saline (PBS), vortexed for 10 min, and stored at 4 °C in the dark. After preparation, test dispersions were immediately used by diluting with *Dulbecco's Modified Eagle Medium (DMEM)*.

2.2. Synthesis of $SiO_2@TiO_2$

Spherical particles with an amorphous, solid core of SiO_2 and a porous, polycrystalline shell of TiO_2 formed in a three-step procedure. The first step yielded silica spheres, the second step produced sphere of silica covered with a layer of amorphous titanium oxide, and the last step crystallized the titanium oxide in the shell with a mild chemical treatment. Synthesis of silica spheres with a narrow distribution in size followed as described in an earlier contribution [31]. Formation of an homogenously thick layer of titanium oxide followed likewise as previously described [32]. We adapted a procedure developed for amorphous gels of TiO_2 to crystallize the shell [33]. Thus, we obtained core@shell spheres with an amorphous, solid core of SiO_2 and a crystalline, porous shell of TiO_2 ($SiO_2@TiO_2$).

The shell crystallized with a mild chemical treatment. First, we poured 16.62 g of ethanol and then 0.083 g of HCl 36.5–38.0% from a glass beaker into a clean round-bottom flask (200 mL, one neck) in a fume hood and closed the flask with a septum. Then, we added 0.500 ± 0.001 g of silica spheres covered with amorphous TiO_2, a magnetic stir bar, and closed again the flask with the septum. We immersed the closed flask in an oil bath until the liquid surface in the flask remained below the liquid surface of the oil. After inserting a metallic needle (outer diameter 2 mm) through the septum, we turned on the heating plate. The temperature in the oil bath rose to 100.0 ± 0.1 °C under slow magnetic stirring. After reaching 100.0 ± 0.1 °C, the flask remained at this temperature 12 h. During this time, the liquid evaporated through the needle and a pale yellow solid appeared inside the flask. Then, we removed the flask from the oil bath and let it cool down to room temperature. After opening the flask, we removed the solid inside from the inner glass wall with a metallic spatula, collected it over a paper sheet, and finally swept it into a glass vial, which we closed with a screw lid.

2.3. Physicochemical characterization of nano- and core@shell-particles

We determined crystalline phases in core@shell spheres with X-ray diffraction (XRD), and final shape and mean particle size of core@shell particles, as well as the remaining shells after selectively dissolving the cores from $SiO_2@TiO_2$ with Scanning Electron Microscopy (SEM). We determined shape and mean particle size of TiO_2-NP from TEM-images and obtained nitrogen adsorption–desorption isotherms at 77 K from samples previously activated under vacuum at 423 K for at least 2 h. We calculated specific surface areas with the Brunauer–Emmett–Teller (BET) method.

2.4. Cell culture

Rat osteosarcoma-derived cells (UMR106) were originally obtained from the American Type Culture Collection (ATCC, CRL 1661, Rockville, MD, USA). Cells were grown as monolayers with DMEM culture medium supplemented with 10% inactivated fetal calf serum, 50 UI mL^{-1} of penicillin and 50 ppm of streptomycin sulfate in a humidified incubator at 37 °C and 5% CO_2 atmosphere. Cells were subcultured using 0.25% trypsin, 1 mM EDTA in phosphate-buffered saline.

2.5. Biocompatibility assays

2.5.1. Cell viability assay

After treatment with different concentrations of TiO_2-NP or $SiO_2@TiO_2$ for 24 h, cells were detached with trypsin and counted

in a Neubauer hemocytometer with the Trypan Blue dye exclusion method.

2.5.2. Cytotoxicity assays

The *Neutral Red* (NR) uptake assay was performed according to Borenfreund and Puerner [34]. Briefly, cells were treated with TiO_2-NP or SiO_2@TiO_2 within the range of 5–100 ppm for 24 h. Following exposure, cells were incubated with 100 ppm NR dye for 3 h. Then, extraction solution was used to fix the cells and release the neutral red into solution. The absorbance at 540 nm was recorded using a Microplate spectrophotometer (7530, Cambridge Technology Inc., USA). Results were expressed as the mean of three independent experiments and plotted as percent of control.

The *MTT* assay was carried out according to Mosmann [35]. Briefly, cells were treated with TiO_2-NP or SiO_2@TiO_2 within the range of 5–100 ppm for 24 h. Following exposure, cells were incubated with 0.5 mg mL^{-1} MTT for 3 h. Cells were lysed in DMSO. Color development was measured at 570 nm. Results were expressed as the mean of three independent experiments and plotted as percent of control.

2.5.3. Cytokinesis-block micronucleus assay

Experiments were set up with cultures in the log phase of growth. UMR106 cells were treated with different concentrations of TiO_2-NP or SiO_2@TiO_2 along with cytochalasin B (4.5 ppm). After 24 h, cells were rinsed and subjected to hypotonic conditions at 37 °C for 5 min, fixed with methanol at −20 °C for 10 min and stained with 5% Giemsa. For the analysis, 500 binucleated (BN) cells were scored at 400× magnification per experimental point from each experiment. The examination criteria employed were reported by Fenech [36].

2.5.4. Assessment of nuclear division index (NDI)

The NDI indicates the mitogenic response of the cells and has also been considered an indicator of cytostatic effects [37]. A minimum of 500 viable cells per experimental point was scored to determine the percentage of cells with one, two, and three or more nuclei. NDI was calculated according to the formula: NDI = $(M_1 + 2M_2 + 3M_3 + 4M_4)/N$, where M_1–M_4 represent the number of cells with one to four nuclei, respectively, and N is the total number of cells analyzed, excluding the necrotic and apoptotic cells.

2.5.5. Single cell gel electrophoresis (Comet assay)

For detection of DNA damage, the Comet assay was employed based on the method of Singh et al. [38] with minor modifications. Briefly, cells were suspended in 0.5% low melting point agarose and immediately poured onto microscope slides precoated with 0.5% normal melting point agarose. Slides were immersed in ice-cold lysis solution (pH 10) for 1 h. Electrophoresis was performed at 25 V in alkaline buffer (pH 12.7). Afterwards, slides were neutralized and stained with SyberGreen. Analysis was performed in an Olympus BX50 fluorescence microscope. A total of 100 randomly captured cells per experimental point were used to determine the tail moment (product of tail length by tail DNA percentage) using Comet Score version 1.5 software.

2.5.6. Uptake and subcellular localization by TEM

After treatment with 50 ppm of TiO_2-NP or SiO_2@TiO_2UMR106, UMR106 cells were fixed in 2% glutaraldehyde for 1 h at 4 °C. Later, cells were treated with 2% OsO_4 in sodium cacodylate and embedded in epoxy resin, Epon (Serva, Heidelberg, Germany). Ultrathin sections (60 nm) were obtained by ultramicrotome (Supernova Reichert-J). These sections were stained with uranyl acetate solution in acetic acid and plumbic citrate. TEM analyses of ultrathin sections allowed determining morphologic characteristics of the shell and distribution of particles within the cells.

2.5.7. Determination of Reactive Oxygen Species (ROS) level

Intracellular ROS were determined by oxidation of *Dihydrorhodamine-123 (DHR-123)* to rhodamine by spectrofluorescence [39]. Briefly, UMR106 cells were incubated at 37 °C with different concentrations of TiO_2-NP or SiO_2@TiO_2. After 24 h, cells were incubated with 10 mM DHR-123 [40]. Cells were scraped into 1 mL 0.1% Triton-X100. Then, the oxidized product was measured with a Perkin–Elmer LS-50B luminescence spectrometer (Beaconsfield, England). Results were corrected for protein content by the method of Bradford [41].

2.6. Statistical analysis

Data are expressed as mean ± standard error of the mean (s). Statistical analysis of the data was carried out by ANOVA followed by the Fisher's Least Significant Difference (LSD) method. The statistical analyses were performed using a computer program (Statgraphics plus 5.1).

3. Results

We estimated shape and mean particle size from TiO_2-NP and SiO_2@TiO_2 from electron microscopy images. The former had an irregular shape, and we estimated their mean particle size from TEM-images (not shown) as reported previously [42]. Briefly, we measured the largest length from each particle to estimate the mean particle diameter, and obtained after 146 measurements a mean particle size of 20 ± 7 nm. The latter particles were spherical and had diameters within a narrow range (Fig. 1). After measuring 40, 100, and 100 diameters in SEM-image from three independently synthesized samples, we calculated following mean particle diameters: 590 ± 30, 580 ± 30, and 510 ± 40 nm.

A shell formed around silica spheres. TEM-images of UMR 106 cells treated with SiO_2@TiO_2 showed spherical particles with a lighter core and a darker shell (Fig. 11). These TEM-images of ultrathin sections (60 nm) evidenced sections of spherical particles having each a darker outer ring and a lighter inner core. We had already observed this contrast between the material at the core and the shell for SiO_2@ZrO_2 [43]. A second evidence of shell formation around silica spheres were broken shells we observed in SEM-images of the remaining material after selectively dissolving the silica core from SiO_2@TiO_2 (Fig. 2).

SiO_2@TiO_2 had nanometer-sized anatase crystals. Before being treated with acidic ethanol, core@shell spheres solely presented a broad reflex extending from below 20 2θ up to ca. 40 2θ attributable to X-ray scattering (Fig. 3). After the mild chemical treatment, core@shell spheres presented a main broad reflex centered at

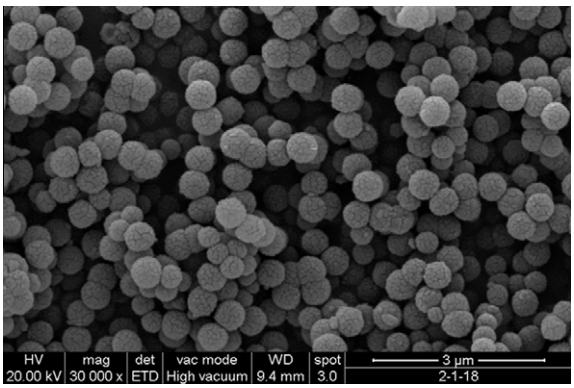

Fig. 1. SiO_2@TiO_2 spheres as seen with SEM. Particles were covered with gold to improve resolution.

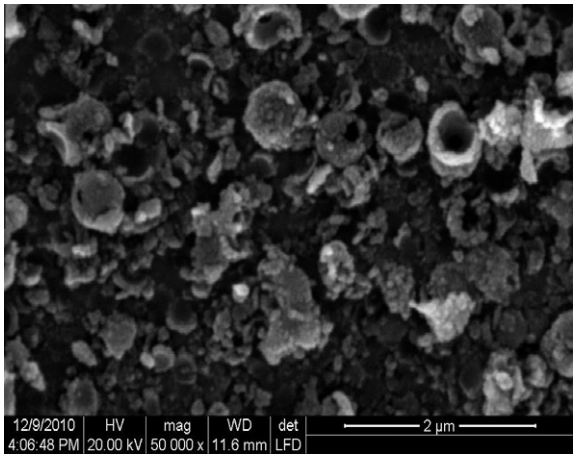

Fig. 2. Fragments from broken shells after removal of core seen with SEM. Particles were covered with gold to improve resolution.

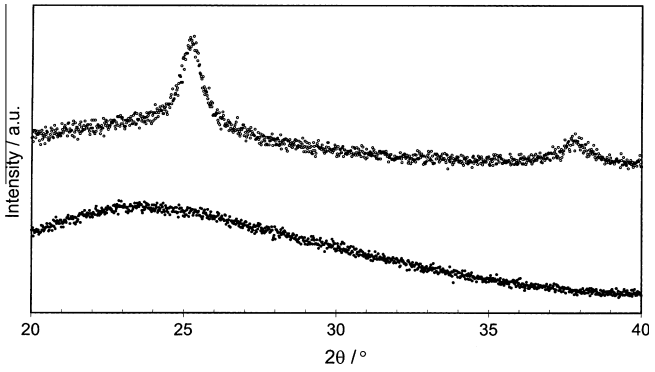

Fig. 3. X-ray diffractograms of SiO_2@TiO_2 before (bottom) and after (top) mild chemical treatment with acidic ethanol. Intensities in ordinate normalized and expressed in arbitrary units. Angles in abscissa expressed in 2θ. Reflexes positioned at 25.2 and 37.8 2θ correspond to planes (101) and (004) of TiO_2 anatase.

25.30 ± 0.01 2θ and a likewise broad though less intense reflex at 37.82 ± 0.01 2θ. We attributed those reflexes to nanometer-sized anatase.

SiO_2@TiO_2 possessed micro and mesopores as well as a specific surface area of ca. 300 $m^2\ g^{-1}$. We obtained nitrogen sorption isotherms for TiO_2-NP, silica spheres covered with an amorphous shell of TiO_2, and three independently synthesized samples of SiO_2@TiO_2. Comparison of isotherms corresponding to silica spheres, silica spheres after formation of the amorphous shell, and core@shell particles after the mild chemical treatment showed the changes introduced in the pore structure of the material after each step of the synthesis pathway. Solid silica spheres before the coating had a characteristic type II isotherms (not shown, see for instance [31]) and low specific surface areas (<10 $m^2\ g^{-1}$). Silica spheres covered with a thin amorphous shell of TiO_2 presented a type IV isotherm with a small hysteresis and adsorbed volumes higher than 100 mL at low relative pressures (Fig. 4). After the mild chemical treatment, SiO_2@TiO_2 had a likewise type IV isotherm, which showed a reduction of the adsorbed nitrogen. This downwards displacement of the isotherm indicated that a reduction of the specific pore volume and a reduction of the specific surface area occurred during the treatment with acidic ethanol. Table 1 shows calculated specific surface areas for TiO_2-NP and core@shell spheres before and after the chemical treatment.

TiO_2-NP and SiO_2@TiO_2 influenced the viability of UMR106 cell according to the Trypan blue assay. TiO_2-NP exerted a decrease in

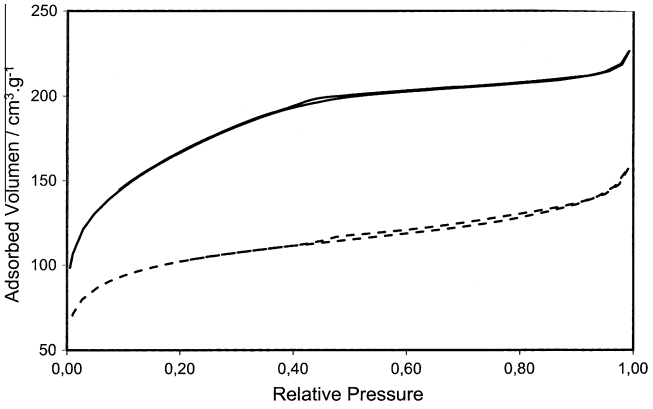

Fig. 4. Nitrogen sorption isotherms obtained for the solid before (top) and after (bottom) the mild chemical treatment.

Table 1
Crystalline phases observed with XRD and specific surface áreas calculated for core@shell spheres before and after mild chemical treatment and TiO_2-NP.

Sample	Crystalline phase	Specific surface area[b] ($m^2\ g^{-1}$)
SiO_2@TiO_2[a]	Non-crystalline	593 ± 89
SiO_2@TiO_2	Anatase	315 ± 47
	Anatase	368 ± 55
	Anatase	211 ± 32
TiO_rNP	Anatase[c]	142 ± 21

[a] Core@shell spheres after formation of homogenous shell of TiO_2 but before its treatment with acidic ethanol.
[b] Error was expressed as value ± s with s equal 15% of the estimated value.
[c] Provided by supplier.

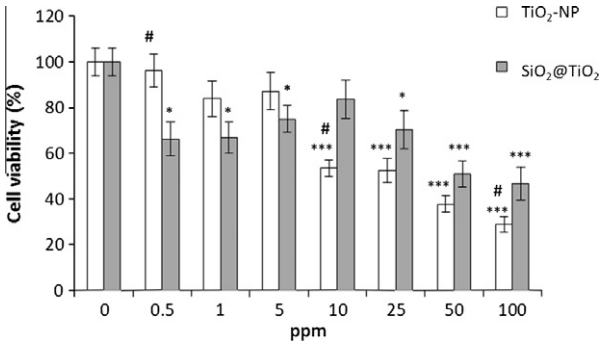

Fig. 5. Effect of TiO_2-NP or SiO_2@TiO_2 on UMR106 cell viability. Cells were incubated in DMEM without (basal) or with different concentrations of the materials (0.5, 1, 5, 10, 25, 50, and 100 ppm) at 37 °C for 24 h. Results are expressed as % basal and represent the mean ± s (standard error of the mean) ($n = 7$), *significant differences versus control, $p < 0.05$, ***significant differences versus control, $p < 0.001$, #significant differences between materials at the same concentration, $p < 0.05$.

UMR106 cell viability in a dose response form (Fig. 5). This effect was statistically significant in relation to basal condition from 10 ppm ($p < 0.001$). On the other hand, SiO_2@TiO_2 triggered a bell-shaped response. In other words, a decrease in cell viability in the range of the low concentrations (0.5–5 ppm, $p < 0.05$) and a second reduction in a concentration-dependent manner from 25 ppm ($p < 0.05$ at 25 ppm and $p < 0.001$ from 50 ppm). In addition, calculated IC_{50} for both TiO_2-NP and SiO_2@TiO_2 quantified their deleterious effect in UMR106 cells. TiO_2-NP (IC_{50} = 30 ppm) more strongly affected the cells than SiO_2@TiO_2 (IC_{50} = 54 ppm). Thus, TiO_2-NP caused a greater decrease in cell viability than SiO_2@TiO_2 in UMR106 cells.

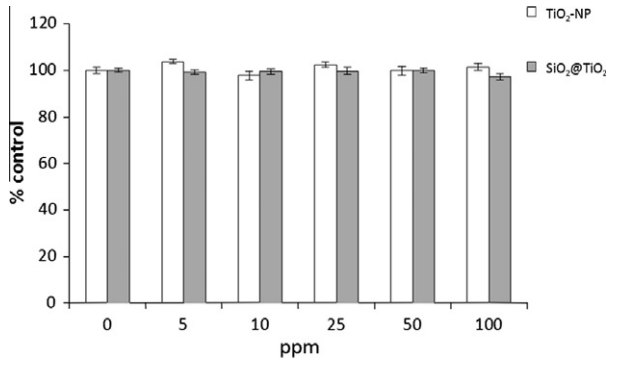

Fig. 6. NR uptake assay in UMR106 cells. After incubation with TiO_2-NP or SiO_2@TiO_2, lysosomal activity was determined by the uptake of NR. The dye taken up by the cells was extracted and the absorbance read at 540 nm. Results are expressed as % basal and represent the mean ± s (standard error of the mean) ($n = 16$), *significant differences versus control, $p < 0.05$, ***significant differences versus control, $p < 0.001$, #significant differences between materials at the same concentration, $p < 0.05$.

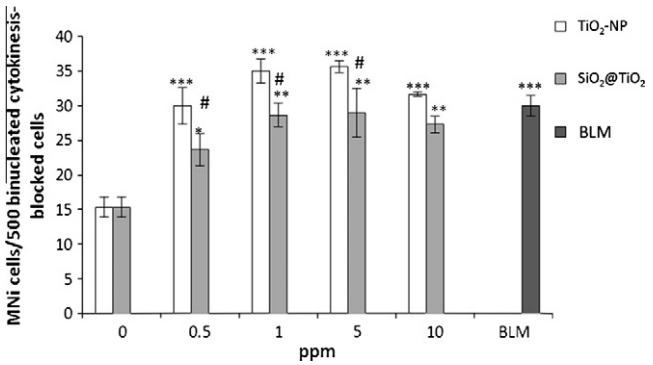

Fig. 8. Micronucleus induction in UMR106 cells after 24 h exposure to TiO_2-NP or SiO_2@TiO_2. Results are presented as mean MNi cells/500 binucleated cytokinesis-blocked cells of pooled data from three independent experiments ± s (standard error of the mean), *significant differences versus control, $p < 0.05$, **significant differences versus control, $p < 0.01$, ***significant differences versus control, $p < 0.001$, #significant differences between materials at the same concentration, $p < 0.05$. BLM, bleomycin (1 μg mL^{-1}, positive control).

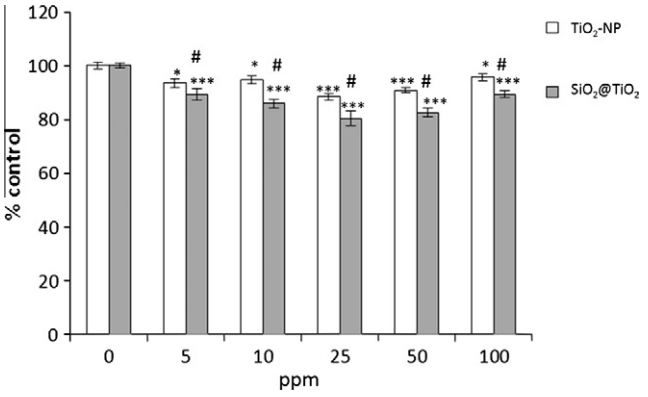

Fig. 7. MTT assay in UMR106 cells. After incubation with TiO_2-NP or SiO_2@TiO_2, mitochondrial activity was determined by the conversion of the tetrazolium salt to a colored formazan by mitochondrial dehydrogenases. Color development was measured at 570 nm after cell lysis in DMSO. Results are expressed as % basal and represent the mean ± s (standard error of the mean) ($n = 16$), *significant differences versus control, $p < 0.05$, ***significant differences versus control, $p < 0.001$, #significant differences between materials at the same concentration, $p < 0.05$.

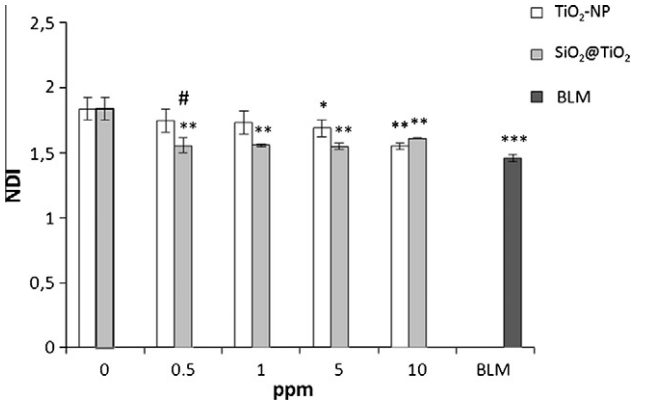

Fig. 9. Nuclear division index (NDI) values for control, TiO_2-NP and SiO_2@TiO_2-treated in binucleated cytokinesis-blocked UMR106 cells. Results are presented as mean value of pooled data from three independent experiments ± s (standard error of the mean), *significant differences versus control, $p < 0.05$, **significant differences versus control, $p < 0.01$, #significant differences between materials at the same concentration, $p < 0.05$. BLM, bleomycin (1 ppm, positive control).

TiO_2-NP and SiO_2@TiO_2 did not alter the lysosomal activity in the concentration range studied (up to 100 ppm) (Fig. 6).

UMR106 cells exposed to dispersions of either TiO_2-NP or SiO_2@TiO_2 with different concentrations (5–100 ppm) reduced the ability of UMR106 cells to form the insoluble violet product (Fig. 7). TiO_2-NP significantly reduced the cell's ability to reduce MTT for concentration values $\geqslant$5 ppm ($p < 0.05$) and 25 ppm ($p < 0.001$). Likewise, SiO_2@TiO_2 inhibited the cell metabolism for concentrations >5 ppm ($p < 0.001$). Even though SiO_2@TiO_2 harmed cells less than TiO_2-NP, SiO_2@TiO_2 still reduced by 80% the ability of cells to reduce MTT.

Two different assays tested genotoxicity of both types of particles: MN assay and Comet assay. The MN assay screens genotoxicity by determining formation of NM (i.e., cytoplasmic bodies having either a portion of an acentric chromosome or the whole chromosome which normally develop a nuclear membrane) [44]. The frequencies of MN in the BLM (positive control) treatment cells significantly increased compared to the control cultures ($p < 0.001$) (Fig. 8). The frequencies of MN in binucleated cells after exposure to either TiO_2-NP or SiO_2@TiO_2 (0.5–10 ppm) for 24 h showed a progressive concentration-related induction of MN for concentrations >5 ppm by TiO_2-NP ($p < 0.001$) and SiO_2@TiO_2 ($p < 0.05$). At the same concentration of particles, TiO_2-NP provoked a significant higher induction of MN than SiO_2@TiO_2.

NDI indicates the vitality of a cell culture undergoing genotoxic treatment, and its value, calculated as shown before, lies between 1 and 2. The NDI index calculated for cultures treated with either TiO_2-NP or SiO_2@TiO_2 was disturbed (Fig. 9). While cells treated with a concentration range of 0.5–1 ppm of TiO_2-NP exhibited a normal rate of nuclear division, cells treated with concentrations either >5 ppm of TiO_2-NP ($p < 0.05$) or >0.5 ppm of SiO_2@TiO_2 ($p < 0.01$) showed a delay in the onset of cell division. At a concentration of 0.5 ppm, SiO_2@TiO_2 delayed the rate of nuclear division more than TiO_2-NP ($p < 0.05$) (Fig. 9).

The Comet assay – second assay aiming determination of genotoxicity – tested the induction of DNA damage after exposing cells to both types of particles. TiO_2-NP induced DNA damage in UMR106 cells from 0.5 to 10 ppm (Fig. 10). At 5 and 10 ppm, Tail Moment was as high as the DNA damage generated by a pulse of 20 min of 1 ppm of bleomycin (positive control in this assay). On the other hand, SiO_2@TiO_2 did not induce DNA damage in UMR106 cells from 0.5 to 5 ppm detected by this assay.

Altogether, both genotoxicity studies showed that TiO_2-NP induced DNA damage and increased MN frequency from 0.5 ppm in UMR106 cells, while SiO_2@TiO_2 only induced MN from 0.5 ppm.

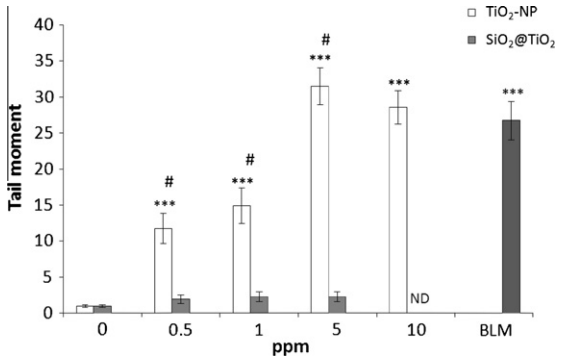

Fig. 10. Comet assay in UMR106 cells after 24 h exposure to TiO_2-NP or SiO_2@TiO_2. Results are presented as mean Tail moment ± s (standard error of the mean), ***significant differences versus control, $p < 0.001$, #significant differences between materials at the same concentration, $p < 0.05$. ND not determined. BLM, bleomycin (1 ppm, positive control).

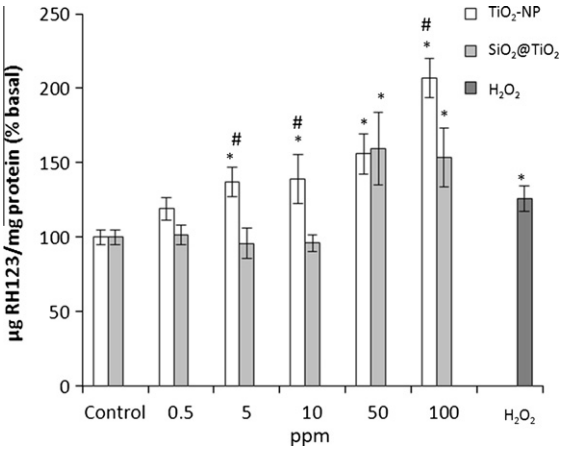

Fig. 12. Induction of ROS by TiO_2-NP or SiO_2@TiO_2 in UMR106 cells. Cells were incubated with growing concentrations of the materials at 37 °C for 24 h. ROS production in the cells was evaluated through the oxidation of DHR-123 to Rhodamine 123 (RH123). Results represent the mean ± s (standard error of the mean) ($n = 6$), *significant differences versus control, $p < 0.05$, #significant differences between materials at the same concentration, $p < 0.05$. H_2O_2 (4 mM, positive control).

UMR106 cells exposed to either TiO_2-NP or SiO_2@TiO_2 (50 ppm) for 24 h showed particles both on the surface and inside the cells (Fig. 11). Cells exposed to TiO_2-NP had a large portion of their outer surface covered with nanoparticles. Moreover, nanoparticles located in all folds and cavities of the cell plasma membrane (Fig. 8C). Agglomerates of TiO_2-NP seemed to have been phagocyted by the cells and included as intracellular vesicles into the cytoplasm. Initial changes in the cell membrane previous to endocytosis could be observed. Interestingly, nanoparticles within the cells situated exclusively in the cytoplasm (Fig. 11C). Cells exposed to SiO_2@TiO_2, on the other hand, incorporated particles in their cytoplasm. However, no membrane-bound vesicles could be distinguished (Fig. 11B).

Possible mechanism of cell death triggered by TiO_2-NP or SiO_2@TiO_2 could be inferred by determining the oxidative stress (i.e., ROS production). TiO_2-NP and SiO_2@TiO_2 induced both a dose-dependent oxidative stress in UMR106 cells with a stronger response for TiO_2-NP (Fig. 12). The oxidative stress produced by both particles differed from the control for >5 ppm TiO_2-NP ($p < 0.05$) and the response at 100 ppm doubled the value of control. On the other side, SiO_2@TiO_2 particles increased ROS production at concentrations >50 ppm ($p < 0.05$). These results suggest that the damage caused by oxidative stress is more pronounced with the smaller particles (i.e., TiO_2-NP).

4. Discussion

This study confirms that colloidal SiO_2@TiO_2 spheres formed in a three-step procedure, being the last step a mild chemical treatment with acidic ethanol. This treatment rearranged the elements from the amorphous shell of TiO_2 into nanocrystal with anatase structure without detaching the shell from the silica core and without losing the shell integrity. SiO_2@TiO_2 spheres presented two main reflexes corresponding to TiO_2 (anatase). The specific surface area dropped from ca. 600 to 300 $m^2\ g^{-1}$ after crystallization, while keeping micro and mesopores. Unexpectedly, this study showed that core@shell spheres as big as 600 nm do harm UMR106 cells though less than TiO_2-NP.

The amorphous shell of TiO_2 in core@shell spheres successfully crystallized with a mild chemical treatment with acidic ethanol. Though crystallization of amorphous titanium oxide with acidic ethanol was reported [33], its suitability for the formation of SiO_2@TiO_2 was unknown. Crystallization of the shell in synthesis pathways reported so far was accomplished with a thermal treatment. These thermal treatments yielded SiO_2@TiO_2 with lower specific surface areas and sometimes mixtures of anatase and rutile polymorphs. In 1996, a synthesis pathway for SiO_2@TiO_2 yielded shells whose thickness ranged from submonolayer to 7-nm [45]. One feature of this procedure is that $Ti(OBu)_4$ and water were mixed before addition to the dispersion containing the silica spheres. A thermal treatment up to 500 °C crystallized the shell, and specific surface areas ranged from 20 to 69 $m^2\ g^{-1}$. Later on, a different pathway proposed to directly inject titanium alkoxyde into a closed flask containing silica spheres dispersed in a solution

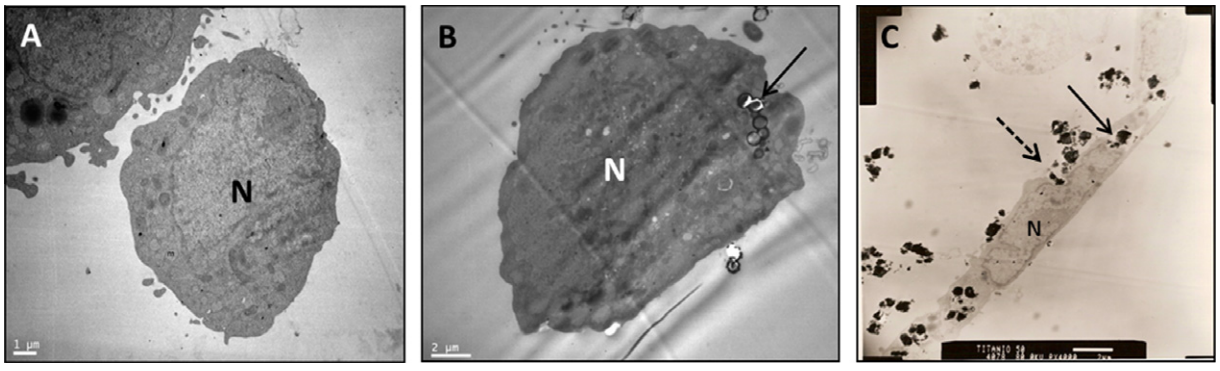

Fig. 11. Transmission electron micrographs of UMR 106 cells treated during 24 h with (A) control, (B) SiO_2@TiO_2 50 ppm, and (C) TiO_2-NP 50 ppm. Intracellular phagocyted material can be observed (black arrows); SiO_2@TiO_2 as free particles (B) and TiO_2-NP within vesicles (C). Initial changes in the cell membrane previous to endocytosis can be observed after treatment with TiO_2-NP (dotted arrow). N: nucleus, m: mitochondria.

of water and Lutensol AO5 in ethanol, and the solid material was aged for 3 days in water before calcination up to 900 °C [43]. Thereafter followed a different approach, where the shell formed after a cyclic deposition process [9] and crystallization was brought about by calcination. This approach produced spheres with rough surfaces having anatase after calcination up to 400–1000 °C and additionally rutile after heating up to 1000 °C. Reported specific surface areas were 107 $m^2 g^{-1}$ (400 °C), 49 $m^2 g^{-1}$ (500 °C), and 44 $m^2 g^{-1}$ (600 °C). Another cyclic coating [46] introduced ultrasound treatments between coatings. Though the first coatings produced single spheres, a threshold number of coatings was found above which spheres coarsed. Irrespective of the number of coatings, particles had rough surfaces and roughness increased with number of coatings. More recently, a protocol previously developed for $SiO_2@ZrO_2$ spheres [43] was adapted to prepare $SiO_2@TiO_2$ spheres [47]. Crystallization of the shell occurred above 800 °C. The thermal treatment provoked a steep reduction of specific surface areas as temperature rose: 205 $m^2 g^{-1}$ (800 °C), 125 $m^2 g^{-1}$ (900 °C), 15 $m^2 g^{-1}$ (1000 °C), and 10 $m^2 g^{-1}$ (1100 °C).

$SiO_2@TiO_2$ spheres have also been prepared with synthesis pathways different than the three-step-approach (i.e., synthesis of template, formation of amorphous shell, and crystallization of shell). In 2006, an article presented a synthesis pathway proposed to build the shell via heterocoagulation from previously synthesized crystalline TiO_2-NP on the surface of silica spheres [48]. Here, the authors claimed to have successfully formed TiO_2 shells from electrophoretic measurements. By the same time, another synthesis pathway proposed to build a composite shell via layer-by-layer deposition and then to crystallize the shell with a thermal treatment up to 450 °C [22]. Unfortunately, the article lacked of XRD-diffractograms and mention to positions of reflexes. More recently, another pathway formed $SiO_2@TiO_2$ via heterocoagulation of TiO_2-NP and silica spheres [49]. Specific surface areas were not reported.

Trypan Blue exclusion assay showed that both $SiO_2@TiO_2$ and TiO_2-NP interfered with the viability of UMR106 osteoblast-like cells cultured *in vitro* (Fig. 5), though differently. On one side, TiO_2-NP affected more cells than $SiO_2@TiO_2$, as inferred from IC_{50} values. Moreover, the cell count decreased in a concentration-dependent manner with a steep reduction at 10 ppm that could be related to the increase in ROS production (Fig. 12). On the other side, $SiO_2@TiO_2$ provoked at first a decrease in cell viability within the range of low concentrations (ca. 70% from 0.5 to 5 ppm) that may be attributed to a delayed rate cell division, indicated by a decrease in the NDI (Fig. 9), and then provoked again a second decrease from 25 ppm, associated with an increase in ROS production (Fig. 12). Therefore, above 10 ppm, TiO_2-NP is more toxic than $SiO_2@TiO_2$ since the oxidative stress induced by TiO_2-NP in UMR106 cells is significantly higher. However, at lower concentrations, there was no increase in ROS production for any material, although $SiO_2@TiO_2$ induced a delay in rate cell division, which triggers a decrease in cell viability. These findings agreed with previous observations where cancer cell lines as well as cultured human cells experienced a decrease in cell viability after exposure to TiO_2-NP [50–52]. In addition, both size and crystal structure of TiO_2 nanoparticles induced a dose-dependent decrease in cell viability of PC12 cells. In contrast, micrometer-sized TiO_2 (hydrodynamic diameter of 25 μm) did not alter cell proliferation [53]. On the other hand, fine rutile TiO_2 (99.9%; particle size <5 μm) reduced cell viability at lower doses than nanosized anatase, which was more cytotoxic than nanosized rutile evaluated in human bronchial epithelial BEAS 2B cells [54]. Cell viability of core@shell materials has been evaluated *in vitro* in different systems. A recent study conducted to assess the biocompatibility of the core–shell Fe_3O_4@-Au composite magnetic nanoparticles showed no cytotoxicity for this material on mouse fibroblast cell line [55]. Altogether, our results suggest that the effect on cell viability is less marked with $SiO_2@TiO_2$ than with TiO_2–NP. The reason for this difference may be attributed to the dissimilarity in size and structure even though the chemical surface is equivalent.

Two well-known methods evaluated cytotoxicity of $SiO_2@TiO_2$ and TiO_2-NP: the NR uptake and the MTT assays. The NR uptake assay showed that UMR106 cells exposed to both TiO_2-NP and $SiO_2@TiO_2$ within the concentration range of 5–100 ppm for 24 h kept their ability to incorporate and bind NR dye. Thus, UMR106 cells were invulnerable to both TiO_2-NP and $SiO_2@TiO_2$, at least when considering the lysosomes as biological targets. In agreement with our results, Reeves et al. [56] reported that TiO_2 nanoparticles alone in a concentration range from 0.1 to 1000 ppm had little effect, whereas coexposure with UVA light was necessary to cause a significant dose-dependent decrease in the incorporation of NR dye. However, fish cells (RTG-2) exposed to 50 ppm TiO_2 nanoparticles over 24 h *in vitro* significantly reduced the lysosomal integrity [57].

The MTT assay, on the other hand, showed that UMR106 cells exposed to low concentrations (from 5 ppm) of either TiO_2-NP or $SiO_2@TiO_2$ experienced a significant reduction in their ability to reduce the MTT dye. It can be highlighted that MTT assay evidenced toxicity when exposing UMR106 cells to TiO_2-NP and $SiO_2@TiO_2$ before any effect with NR assay could be detected. This behavior could be attributed to the eventual effect of the particles on mitochondria previous to any disruption on lysosomal activity. In agreement with our results, mouse fibroblasts (L929 cells) treated with TiO_2 nanoparticles showed concentration-dependent cytotoxicity, with drastic changes at high concentrations (>6 ppm) [58]. Furthermore, exposing rat liver cells to doses of TiO_2 in the range 10–50 ppm had no measurable effect, but exposition to higher doses (100–250 ppm) showed measurable effects [59]. Moreover, TiO_2-NP produced a concentration-dependent cytotoxic effect evaluated by the NR and MTT assays on human hepatocellular carcinoma, Hep-G2 cells [60], and on human amnion epithelial (WISH) cells in a concentration range of 0.625–10 ppm [30]. Consequently, cytotoxic effect has shown to depend on concentration of particles, composition of particles, and cell line.

Furthermore, uptake and defense mechanism may considerably differ among different types of cells [60]. Biomolecules (e.g., proteins, natural organic molecules, enzymes) immediately cover nanoparticles upon entrance into a biological medium [30]. Thus, the biomolecule "corona" constitutes the primary contact to the cells [61], which may lead to a different *in vivo* response than an uncoated particle. More specifically, the effect of the same nanoparticles on several cells is significantly different and could not be assumed for other cells; the possible mechanisms relate to the different detoxification strategies that any particular cell can employ in response to nanoparticles. Thus, what the cell "sees" when it is faced with nanoparticles, most likely depend on the cell type [60,62].

As processes responsible for genotoxicity may start before the alterations at the cytoplasm level can be detected, MN assay and comet assay investigated the effect of TiO_2-NP and $SiO_2@TiO_2$ at the nuclear level. MN frequency in UMR106 cells increased after exposure to TiO_2-NP and $SiO_2@TiO_2$. Both materials induced genetic damage at concentrations as low as 0.5 ppm. However, TiO_2-NP induced a stronger and statistically different response than $SiO_2@TiO_2$. These findings are in agreement with previous studies demonstrating that nanoparticle increased MN frequencies in cultured lymphoblastoid cells [51] and Syrian hamster embryo fibroblasts [63]. The comet assay under alkaline conditions detects single and double strand breaks as well as abasic sites (i.e., sites missing either a pyrimidine or purine nucleotide). Here, TiO_2-NP produced a significant genotoxic effect that could be observed from 0.5 ppm, while no DNA damage could be detected in UMR106 cells exposed to $SiO_2@TiO_2$ by this assay.

Genotoxicity may depend on particle size [64]. Nano-TiO_2 more actively induced micronuclei and nucleoplasmic bridges in blood cells than micro-TiO_2. Besides, nanosized anatase elevated the frequency of micronucleated human bronchial epithelial, BEAS 2B cells and induced DNA damage more efficiently than fine rutile TiO_2 or SiO_2-coated nanosized rutile TiO_2 [54]. Moreover, agglomeration of nanoparticles and different dispersion methods (e.g., different periods of sonication) of TiO_2 nanoparticles wund DNA in human cells *in vitro* differently [65]. Scarce information about the genotoxicity of core@shell particles is available. For example, Fe_3O_4@Au composite magnetic nanoparticles did not induce MN formation in L929 [55].

In our case, TiO_2-NP may induce single and double strand DNA breaks in UMR106 cells, which produces a positive result in the Comet assay and induction in micronuclei frequency. However, a positive result from the MN test along with a negative result from the Comet assay suggests that micronucleus formation by SiO_2@TiO_2 might be the result of a disturbance around the mitotic apparatus which might have affected the division process in the cells leading to chromosome loss rather than chromosome rupture.

Furthermore, titanium dioxide nanoparticles seemed to induce ROS-mediated genotoxicity in mammalian cells. It has been shown that TiO_2 nanoparticles generated high levels of DNA adduct formation (detection of 8-hydroxyl-2-deoxyguanosine), associated with ROS generation in human lung cells [66]. Radicals produced under oxidative stress conditions are known to induce a variety of lesions in DNA including strand breaks [67]. Gurr et al. [68] have shown that TiO_2 nanoparticles induce hydrogen peroxide and nitric oxide generation leading to lipid peroxidation and oxidative DNA damage in lung epithelial cells. Finally, a significant induction in micronucleus formation as well as in DNA damage observed by the Fpg-modified Comet assay in human epidermal cells was observed by 0.8 ppm TiO_2 nanoparticles [69].

On the other hand, micronucleus formation has been suggested as the result of physical disturbance of particles around the mitotic apparatus [70]. There is clear evidence that mineral fibers induce chromosomal mutations (aneuploidy and aberrations) in a wide variety of mammalian cells including mesothelial cells [71]. Possible cellular and molecular mechanisms have been proposed [72,73]. A size-dependent mechanism sustains that phagocytized fibers accumulate in the perinuclear region of the cells. When the cell undergoes mitosis, the physical presence of the fibers interferes with chromosome segregation and results in aneuploidy and other chromosome abnormalities. Hence, the physical presence of SiO_2@TiO_2 inside UMR106 cells (detected by TEM) might have affected the division process in the cells leading to chromosome loss and micronuclei induction.

Both types of particles delayed the rate of cell division in UMR106 according to NDI. TiO_2-NP altered the NDI from 5 ppm, fact that can be associated with the increment in the oxidative stress. Moreover, induction of apoptosis and G2/M cell cycle arrest in PC12 cells were linked to ROS induction after exposure to TiO_2 nanoparticles [53]. SiO_2@TiO_2 delayed the onset of cell division from 0.5 to 10 ppm. This delay had no connection to a rise in ROS production. Nevertheless, this delayed rate cell division may explain the decrease in UMR106 cell viability at lower concentrations observed for the Trypan Blue exclusion assay, so as we have previously reported for a concentration-dependent inhibition of UMR106 cell division treated with TiO_2 and Al_2O_3 nanoparticles [74].

Regarding uptake and subcellular localization, TiO_2-NP and SiO_2@TiO_2 particles placed inside and outside the cell. Exposing UMR106 cells to TiO_2-NP during 24 h provoked formation of vesicles and seemed to alter cells and their nuclei (Fig. 11C). UMR106 cells treated with SiO_2@TiO_2, on the other hand, displayed fewer particles in the cytoplasm, and no membrane-bound vesicles could be distinguished (Fig. 11B). Our results agreed with previous observations. Aggregates of TiO_2-NP particles with diameters of 50 nm were found in A549 cell culture (alveolar epithelia type II cells) [75]. Anatase and rutile clusters accumulated in cytoplasm and cytoplasmic vacuoles in HaCaT cells [76]. Anatase nanoclusters (20–30 nm diameter) appeared in L929 mouse fibroblast cells treated for 48 h. In all cases, an increment in the number of lysosomes and the disappearance of some cytoplasmic organelles could be observed [58]. The internalization of particles exclusively in the cytoplasm has been also observed with other particles and cells different from those used in this study. In accordance with flow cytometric analyses performed in mammalian cells with TiO_2 nanoparticles [77], several types of nanoparticles internalized into cells are often found within intracellular vesicles. TEM photographs showed that the vesicles with individual particles and aggregates remained in the cytoplasm, but not in the nucleus. This phenomenon was observed for vascular endothelial cells treated with metal oxide nanoparticles [78] and human pneumocytes [79].

Internalization of particles in UMR106 cells may proceed via pinocytosis, which is fluid-phase endocytosis mechanism that occurs when nanoparticles bind to negatively-charged cell membranes and could lead to the formation of clusters in the vesicles [77,80]. This phenomenon may explain the particle aggregation inside the vesicles and their internalization arranged in perinuclear fashion observed in the present investigation.

Cellular uptake into cells has been shown to depend on particle size. Micro- and nanoparticles made from cationic, cross-linked poly(ethylene glycol) hydrogels internalized in Hela cells with internalization kinetics depending on the absolute size and/or volume of the particle. A possible explanation for this behavior is that multivalent cationic interactions with cells are available with the higher-aspect-ratio particles, because of the larger surface areas in contact with the cell membrane [81]. Similarly, it has been reported that the mechanism of cellular uptake of gold nanoparticles depends on their size and shape as well as on the cell line used in the test [82]. In this regard, our previous results showed a different response between UMR106 and CHO-K1 cells exposed to the same nanoparticles [42,74].

Oxidation of DHR-123 monitored formation of ROS in an attempt to gain deeper insight in the mechanism involved in the cytotoxicity of TiO_2-NP and SiO_2@TiO_2 to osteoblast like cells. TiO_2 nanoparticles disrupted mitochondrial function by the formation of ROS in several cell types such as bronchial epithelial cells, brain microglia, and peripheral lymphocytes [83–85]. TiO_2-NP and SiO_2@TiO_2 induced an oxidative stress in UMR106 cells, though nanoparticles at lower concentration than the spherical particles. TiO_2-NP increased ROS production at low concentrations (5 ppm), which may explain its toxic action associated with mitochondrial injury from 5 ppm (MTT assay) or with the decrease in cell viability from 10 ppm (Trypan Blue assay). SiO_2@TiO_2, on the other hand, increased ROS production in UMR106 osteoblasts from 50 ppm. These results may elucidate the decrease in cell viability at higher concentrations induced by this material. To accord with these findings, it was reported that titanium oxide shell coatings decreased the toxicity of nano-ZnO in parallel with a decrease in intercellular reactive oxygen species [86]. ROS induced by TiO_2 nanoparticles may up-regulate JNK and P53 phosphorylation, which in turn can induce apoptosis and cell cycle arrest in PC12 cells [87]. Moreover, particle size correlated with oxidative stress, and nano-sized TiO_2 produced more ROS than microsized-TiO_2. Anatase TiO_2 nanoparticles generated significant higher levels of ROS at 200 ppm, while micro TiO_2 produced a slight increase.

The toxicity of TiO_2 nanoparticles on different living organisms may depend on exposure to electromagnetic radiation [88–91]. Under UV light for periods of a few minutes, TiO_2 nanostructures were more cytotoxic toward HeLa cells [88]. Moreover, TiO_2 nano-

particles suppressed growth of aquatic biofilm due to the generation of H_2O_2 in the vicinity of the TiO_2-biofilm interfaces [90]. Furthermore, the photocatalytic cancer cell-killing activity of metallic Au-capped TiO_2 (Au@TiO_2) composite colloidal nanopellets investigated on HeLa cells under UV–visible light irradiation has been associated not only to the hydroxyl radical formation, but also to the Au-plasmonic photothermal heat generation [89]. Likewise, TiO_2 nanoparticles were toxic to Daphnia similis only under UV A light, which indicates a toxicity mechanism caused by ROS generation [91].

ROS may generate at the interface between particles and cells. Oxidative stress produced by nanoparticles inside the cell correlates with the BET surface area and the internalized amount [77]. Contrarily, our results showed the opposite behavior. TiO_2-NP with a specific surface area of 142 ± 28 m^2 g^{-1} increased ROS production from 5 ppm, while SiO_2@TiO_2 with a specific surface area of 298 ± 79 m^2 g^{-1} increased ROS from 50 ppm. Interestingly, from the ca. 300 m^2 g^{-1} estimated with the BET method for the core@shell spheres as a whole, only ca. 10 m^2 g^{-1} corresponded to the outer surface – this can be estimated from the geometry and composition of the material. Over 90% of the surface in core@shell particles was inside of the shell. If we consider the specific surface area corresponding to the outer surface of the core@shell spheres, we may conclude that the above mentioned correlation held. Only the outer surface of the material can directly interact with the surface of the cell.

Our results lead to the conclusion that crystallization of the amorphous shell of TiO_2 into anatase nanocrystals brought about with a mild chemical treatment allowed a crystallization of the shell. Despite being the specific surface area high, their values reduced 50% during crystallization. The specific surface area of the SiO_2@TiO_2 may reach higher values than those obtained in this work after thoughtful modification of the experimental variable of synthesis.

5. Conclusions

Altogether, we presented a new synthesis pathway for SiO_2@-TiO_2 and a comparative study on cyto- and genotoxic effects of SiO_2@TiO_2 and TiO_2–NP in rat osteosarcoma (UMR106) cells. To do so, we developed a new method for the synthesis of titanium oxide-coated silica spherical particles. Our overall results showed the ability of these two materials to induce both genotoxicity and cytotoxicity *in vitro*. Both were found inside the cells forming vesicles; however, none of them entered the nucleus. On one hand, TiO_2-NP reduced cell viability from 10 ppm associated with an increase in ROS formation and induction of DNA damage (Comet and MN assays). Alternatively, in SiO_2@TiO_2 exposed cells, there was a cell viability reduction at higher concentrations (above 25 ppm) accompanying with an increase in ROS production. At lower concentrations, the slight decline of cell viability might be related with a delayed rate cell division. Overall, our results suggest that SiO_2@-TiO_2 are less toxic than their nanoparticle counterpart, although this new synthesized material present higher surface area. Further studies are required in order to analyze the mechanisms behind the effects observed.

Acknowledgments

This study was partially supported by a grant from a special research opportunity from the Inter-American Collaboration in Materials Research (CIAM) (ID 372140 & D1032), Centro de Tecnología de Recursos Minerales y Cerámica (CETMIC), and by ANPCyT (PICT 2010-0981). The authors wish to thanks Prof. Dr. Ferdi Schüth at MPI KoFo for providing TiO_2-NP and its characterization by nitrogen sorption and TEM. Dr. Ana Laura Di Virgilio and Dr. Pablo M. Arnal are members of CONICET Argentina.

References

[1] P. Rivera Gil, G. Oberdörster, A. Elder, V. Puntes, W.J. Parak, ACS Nano 4 (2010) 5527.
[2] J. Jang, Adv. Polym. Sci. 199 (2006) 189.
[3] J. Ando, K. Fujita, Curr. Pharm. Biotechnol. Epub ahead of print, 2012.
[4] M. Elsabahy, K.L. Wooley, Chem. Soc. Rev. 41 (2012) 2545.
[5] Z. Zhao, Y. Han, Lin C, D. Hu, F. Wang, X. Chen, Z. Chen, N. Zheng, Chem. Asian J. Epub ahead of print, 2012.
[6] A. Fujishima, X. Zhang, D.A. Tryk, Surf. Sci. Rep. 63 (2008) 515.
[7] R.W. Matthews, Water Res. 20 (1986) 569.
[8] P. Wilhelm, D. Stephan, J. Photochem. Photobiol., A 185 (2007) 19.
[9] S.H. Lim, N. Phonthammachai, S.S. Pramana, T.J. White, Langmuir 24 (2008) 6226.
[10] K. Donaldson, D. Brown, A. Clouter, R. Duffin, W. MacNee, L. Renwick, L. Tran, V. Stone, J. Aerosol Med. 15 (2002) 213.
[11] V. Stone, J. Shaw, D.M. Brown, W. Macnee, S.P. Faux, K. Donaldson, Toxicol. in Vitro 12 (1998) 649.
[12] G. Oberdörster, Int. Arch. Occup. Environ. Health 74 (2001) 1.
[13] T.J. Brunner, P. Wick, P. Manser, P. Spohn, R.N. Grass, L.K. Limbach, A. Bruinink, W.J. Stark, Environ. Sci. Technol. 40 (2006) 4374.
[14] A. Nel, T. Xia, L. Mädler, N. Li, Science 311 (2006) 622.
[15] A. Petushkov, J. Intra, J.B. Graham, S.C. Larsen, A.K. Salem, Chem. Res. Toxicol. 22 (2009) 1359.
[16] E.M. Ophus, L. Rode, B. Gylseth, Scand. J. Work Environ. Health 5 (1979) 290.
[17] R.C. Lindenschmidt, K.E. Driscoll, M.A. Perkins, J.M. Higgins, J.K. Maurer, K.A. Belfiore, Toxicol. Appl. Pharmacol. 102 (1990) 268.
[18] Y. Nakagawa, S. Wakuri, K. Sakamoto, N. Tanaka, Mutat. Res. 394 (1997) 125.
[19] P.J. Lu, I.C. Ho, T.C. Lee, Mutat. Res. 414 (1998) 15.
[20] T. Uchino, H. Tokunaga, M. Ando, H. Utsumi, Toxicol. in Vitro 16 (2002) 629.
[21] R.R. Zhu, S.L. Wang, J. Chao, D.L. Shi, R. Zhang, X.Y. Sun, S.D. Yao, Sci. Eng. C Mater. Biol. Appl. 29 (2009) 691.
[22] H. Nakamura, M. Ishii, A. Tsukigase, M. Harada, H. Nakano, Langmuir 22 (2006) 1268.
[23] M. Holgado, A. Cintas, M. Ibisate, C.J. Serna, C. López, F. Meseguer, J. Colloid, Interface Sci. 229 (2000) 6.
[24] A. Banasik, A. Lankoff, A. Piskulak, K. Adamowska, H. Lisowska, A. Wojcik, Environ. Toxicol. 20 (2005) 402.
[25] A. Lankoff, A. Banasik, A. Duma, E. Ochniak, H. Lisowska, T. Kuszewski, S. Góźdź, A. Wojcik, Toxicol. Lett. 161 (2006) 27.
[26] P.J. Lu, I.C. Ho, T.C. Lee, Mutat. Res., Genet. Toxicol. Environ. Mutagen. 414 (1998) 15.
[27] S. Hackenberg, A. Scherzed, M. Kessler, S. Hummel, A. Technau, K. Froelich, C. Ginzkey, C. Koehler, R. Hagen, N. Kleinsasser, Toxicol. Lett. 201 (2011) 27.
[28] O. Akhavan, E. Ghaderi, A. Akhavan, Biomaterials 33 (2012) 8017.
[29] M.P. Monopoli, D. Walczyk, A. Campbell, G. Elia, I. Lynch, F. Baldelli Bombelli, K.A. Dawson, J. Am. Chem. Soc. 133 (2011) 2525.
[30] M. Mahmoudi, I. Lynch, M.R. Ejtehadi, M.P. Monopoli, F.B. Bombelli, S. Laurent, Chem. Rev. 111 (2011) 5610.
[31] P.M. Arnal, C. Weidenthaler, F. Schueth, Chem. Mater. 18 (2006) 2733.
[32] P.M. Arnal, The Synthesis of Monodisperse Colloidal Core@Shell Spheres and Hollow Particles, Ruhr Universität Bochum, Bochum, Doktor der Naturwissenschaften, 2006.
[33] D.P. Serrano, G. Calleja, R. Sanz, P. Pizarro, J. Mater. Chem. 17 (2007) 1178.
[34] E. Borenfreund, J.A. Puerner, Toxicol. Lett. 24 (1985) 119.
[35] T. Mosmann, J. Immunol. Methods 65 (1983) 55.
[36] M. Fenech, Mutat. Res. 455 (2000) 81.
[37] M. Fenech, Nat. Protoc. 2 (2007) 1084.
[38] N.P. Singh, M.T. McCoy, R.R. Tice, E.L. Schneider, Exp. Cell Res. 175 (1988) 184.
[39] J.A. Royall, H. Ischiropoulos, Arch. Biochem. Biophys. 302 (1993) 348.
[40] C.M. Krejsa, S.G. Nadler, J.M. Esselstyn, T.J. Kavanagh, J.A. Ledbetter, G.L. Schieven, J. Biol. Chem. 272 (1997) 11541.
[41] M.M. Bradford, Anal. Biochem. 72 (1976) 248.
[42] A.L. Di Virgilio, M. Reigosa, P.M. Arnal, M. Fernández Lorenzo de Mele, J. Hazard. Mater. 177 (2010) 711.
[43] P.M. Arnal, The Synthesis of Monodisperse Colloidal Core@Shell Spheres and Hollow Particles, Ruhr-Universität Bochum, Bochum, 2006.
[44] H. Stopper, S.O. Müller, Toxicol. in Vitro 11 (1997) 661.
[45] A. Hanprasopwattana, S. Srinivasan, A.G. Sault, A.K. Datye, Langmuir 12 (1996) 3173.
[46] J.W. Lee, M.R. Othman, Y. Eom, T.G. Lee, W.S. Kim, J. Kim, Microporous Mesoporous Mater. 116 (2008) 561.
[47] P.A. Bazula, Nanostructured Oxidic Materials: Properties and Application of Core@Shell Spheres and Hollow Particles, Ruhr Universitaet Bochum, Bochum, Doktor der Naturwissenschaften, 2010.
[48] P. Wilhelm, D. Stephan, J. Colloid, Interface Sci. 293 (2006) 88.
[49] D.P. Wang, H.C. Zeng, Chem. Mater. 21 (2009) 4811.
[50] P. Thevenot, J. Cho, D. Wavhal, R.B. Timmons, L. Tang, Nanomedicine 4 (2008) 226.
[51] J.J. Wang, B.J.S. Sanderson, H. Wang, Mutat. Res. 628 (2007) 99.
[52] M. Simon, P. Barberet, M.H. Delville, P. Moretto, H. Seznec, Nanotoxicology 5 (2011) 125.

[53] J. Wu, J. Sun, Y. Xue, Toxicol. Lett. 199 (2010) 269.
[54] G.C.M. Falck, H.K. Lindberg, S. Suhonen, M. Vippola, E. Vanhala, J. Catalán, K. Savolainen, H. Norppa, Hum. Exp. Toxicol. 28 (2009) 339.
[55] Y. Li, J. Liu, Y. Zhong, J. Zhang, Z. Wang, L. Wang, Y. An, M. Lin, Z. Gao, D. Zhang, Int. J. Nanomedicine 6 (2011) 2805.
[56] J.F. Reeves, S.J. Davies, N.J.F. Dodd, A.N. Jha, Mutat. Res. 640 (2008) 113.
[57] W.F. Vevers, A.N. Jha, Ecotoxicology 17 (2008) 410.
[58] C.Y. Jin, B.S. Zhu, X.F. Wang, Q.H. Lu, Chem. Res. Toxicol. 21 (2008) 1871.
[59] S.M. Hussain, K.L. Hess, J.M. Gearhart, K.T. Geiss, J.J. Schlager, Toxicol. in Vitro 19 (2005) 975.
[60] M. Mahmoudi, S.N. Saeedi-Eslami, M.A. Shokrgozar, K. Azadmanesh, M. Hassanlou, H.R. Kalhor, C. Burtea, B. Rothen-Rutishauser, S. Laurent, S. Sheibani, H. Vali, Nanoscale 4 (2012) 5461.
[61] D. Walczyk, F.B. Bombelli, M.P. Monopoli, I. Lynch, K.A. Dawson, J. Am. Chem. Soc. 132 (2010) 5761.
[62] S. Laurent, C. Burtea, C. Thirifays, U.O. Häfeli, M. Mahmoudi, PLoS ONE 7 (2012) e29997.
[63] Q. Rahman, M. Lohani, E. Dopp, H. Pemsel, L. Jonas, D.G. Weiss, D. Schiffmann, Environ. Health Perspect. 110 (2002) 797.
[64] L.V. Akhal'tseva, N.E. Moshkov, F.I. Ingel, N.A. Iurtseva, V.V. Iurchenko, Gig. Sanit. (2011) 61.
[65] Z. Magdolenova, D. Bilaniová, G. Pojana, L.M. FjellsbØ, A. Hudecova, K. Hasplova, A. Marcomini, M. Dusinska, J. Environ. Monit. 14 (2012) 455.
[66] K. Bhattacharya, M. Davoren, J. Boertz, R.P.F. Schins, E. Hoffmann, E. Dopp, Part. Fibre Toxicol. 6 (2009).
[67] M.K. Shigenaga, B.N. Ames, Free Radic. Biol. Med. 10 (1991) 211.
[68] J.R. Gurr, A.S.S. Wang, C.H. Chen, K.Y. Jan, Toxicology 213 (2005) 66.
[69] R.K. Shukla, V. Sharma, A.K. Pandey, S. Singh, S. Sultana, A. Dhawan, Toxicol. in Vitro 25 (2011) 231.
[70] T.W. Hesterberg, C.J. Butterick, M. Oshimura, A.R. Brody, J.C. Barrett, Cancer Res. 46 (1986) 5795.
[71] J.C. Barrett, P.W. Lamb, R.W. Wiseman, Environ. Health Perspect. 81 (1989) 81.
[72] C. Walker, J. Everitt, E. Barrett, Am. J. Ind. Med. 21 (1992) 253.
[73] C. Manning, V. Vallyathan, B. Mossman, Int. Immunopharmacol. 2 (2002) 191.
[74] A.L. Di Virgilio, M. Reigosa, M.F. Lorenzo De Mele, J. Biomed. Mater. Res. A 92 (2010) 80.
[75] R.C. Stearns, J.D. Paulauskis, J.J. Godleski, Am. J. Respir. Cell Mol. Biol. 24 (2001) 108.
[76] C. Jin, Y. Tang, F.G. Yang, X.L. Li, S. Xu, X.Y. Fan, Y.Y. Huang, Y.J. Yang, Biol. Trace Elem. Res. 141 (2011) 3.
[77] H. Suzuki, T. Toyooka, Y. Ibuki, Environ. Sci. Technol. 41 (2007) 3018.
[78] A. Gojova, B. Guo, R.S. Kota, J.C. Rutledge, I.M. Kennedy, A.I. Barakat, Environ. Health Perspect. 115 (2007) 403.
[79] A. Simon-Deckers, B. Gouget, M. Mayne-L'Hermite, N. Herlin-Boime, C. Reynaud, M. Carrière, Toxicology 253 (2008) 137.
[80] R. Shukla, V. Bansal, M. Chaudhary, A. Basu, R.R. Bhonde, M. Sastry, Langmuir 21 (2005) 10644.
[81] S.E.A. Gratton, P.A. Ropp, P.D. Pohlhaus, J.C. Luft, V.J. Madden, M.E. Napier, J.M. DeSimone, Proc. Natl. Acad. Sci. USA 105 (2008) 11613.
[82] B.D. Chithrani, W.C.W. Chan, Nano Lett. 7 (2007) 1542.
[83] E.J. Park, J. Yi, K.H. Chung, D.Y. Ryu, J. Choi, K. Park, Toxicol. Lett. 180 (2008) 222.
[84] T.C. Long, J. Tajuba, P. Sama, N. Saleh, C. Swartz, J. Parker, S. Hester, G.V. Lowry, B. Veronesi, Environ. Health Perspect. 115 (2007) 1631.
[85] J.K. Su, M.K. Byeong, J.L. Young, W.C. Hai, Environ. Mol. Mutagen. 49 (2008) 399.
[86] I.L. Hsiao, Y.J. Huang, Chem. Res. Toxicol. 24 (2011) 303.
[87] J. Wu, J. Sun, Y. Xue, Toxicol. Lett. 199 (2010) 269.
[88] J. Chen, H. Zhou, A.C. Santulli, S.S. Wong, Chem. Res. Toxicol. 23 (2010) 871.
[89] M. Abdulla-Al-Mamun, Y. Kusumoto, T. Zannat, M.S. Islam, Phys. Chem. Chem. Phys. 13 (2011) 21026.
[90] P. Dhandapani, S. Maruthamuthu, G. Rajagopal, J. Photochem. Photobiol., B 110 (2012) 43.
[91] G.P.S. Marcone, Á.C. Oliveira, G. Almeida, G.A. Umbuzeiro, W.F. Jardim, J. Hazard. Mater. 211–212 (2012) 436.